Journal of Hydroscience and Hydraulic Engineering
Vol.21, No.1 May, 2003, 11-21

STUDY ON GENERATION MECHANISM OF SECONDARY CURRENTS IN OPEN-CHANNEL FLOW BY DIRECT NUMERICAL SIMULATION

By

Terunori Ohmoto

Associate Professor, Department of Civil and Environmental Engineering,
Kumamoto University, 2-39-1 Kurokami, Kumamoto, Japan

and

Shunichiro Hayashi

Department of Civil Engineering, Kumamoto Prefectural Government,
6-18-1 Suizenji, Kumamoto, Japan

SYNOPSIS

A fully developed three-dimensional turbulent flow over sand ribbons in an open-channel was computed to clarify the generation mechanism of "secondary currents of Prandtle's second kind" by using direct numerical simulation (DNS) with a regular grid in a generalized curvilinear coordinate system. Stable secondary currents and turbulent characteristics were reasonably reproduced. Detailed evaluation of each term in the mean vorticity transport equation revealed that the secondary currents were generated principally by cross-planar turbulent shear stress $(-\overline{v^+ w^+})$ and that the anisotropy of the cross-planar turbulent normal stresses $(\overline{v^{+2}} - \overline{w^{+2}})$ restrained the generation of the secondary currents, where v^+ and w^+ represent vertical and spanwise velocity fluctuations normalized by friction velocity(u_τ) respectively and the overbar denotes time average.

INTRODUCTION

Turbulent shear flow frequently exhibits a pattern of longitudinal stripes such as curl clouds in the atmosphere, Langmuir circulations in oceans, longitudinal dunes parallel to the wind direction in deserts and riverbeds with longitudinal ridges. A predominant factor in these phenomena is a cluster of longitudinal vortices in the flow direction that are cross-sectionally aligned in parallel at a spacing approximately double the thickness of the boundary layer. In rivers, a cluster of longitudinal vortices at a scale of flow depth causes

the positions of maximum velocity to draw down below the free surface and to transform regularly sand wave, bed load and suspended load transversely. Such vortices have considerable the flow resistance law, convective diffusion of heat or materials, and flows around hydraulic structures and thus cause engineering problems in quantitative evaluation. In fluid mechanics, secondary currents are known as "secondary currents of Prandtl's second kind" caused by the anisotropy of turbulence in a straight open channel with a non-circular cross section. A number of studies have been made on the generation mechanisms of secondary currents [1]. Experimental studies have reviewed the convection term, production term and viscosity term in a balance equation for a time-averaged longitudinal vortex in the flow direction [2]. The studies, however, fall short of clarifying the generation mechanism of secondary currents because the terms were extremely small in quantities, and because accuracy was limited to second-order spatial differential operators that were applied to the data obtained by measurements .

Subsequently, with recent advancements in computer technologies, new tools for identifying turbulence phenomena have been developed. In particular, a numerical analysis method called direct numerical simulation (DNS) that is based only on physical laws without any turbulent model is expected to be very useful because of the reliability of the governing Navier-Stokes equations. Also, DNS can explain instantaneous turbulent structures and easily compute high-order statistical data of turbulence. It thus enables the provision of data unobtainable by conventional time-averaged turbulent models or experimental measurements. DNS is expected to make great contributions to the understanding and clarification of turbulence phenomena including the generation mechanism of secondary currents [6].

No DNS studies related to riverbeds with longitudinal ridges, however, have been conducted. The objective of this study is to clarify the generation mechanisms of secondary currents formed in an open channel flow over a riverbed with longitudinal ridges and to examine the effects of the secondary currents on the Reynolds shear stress by using DNS.

FLOW CONFIGURATION AND COMPUTATIONAL PROCEDURE

Computations were carried out for a fully developed turbulent flow in a straight open channel over a riverbed with longitudinal ridges. The bottom shape and the bed height were assumed as shown in Fig. 1 as based on the longitudinal ridges developed from a flat bed [12]. Periodic boundary conditions were applied in the streamwise and the spanwise directions, and the flow field was free from side wall effects.

As the governing equations, the Navier-Stokes equations and the Poisson equation for pressure, both of which were transformed into a three-dimensional generalized coordinate system, were used as shown in equations(1) and (2) below, respectively. Other computational conditions and algorithm used are shown in Table 1 and previous papers [3]-[5].

$$\frac{\partial u_i}{\partial t}+u_j\frac{\partial \xi_k}{\partial x_j}\frac{\partial u_i}{\partial \xi_k}=-\frac{\partial \xi_j}{\partial x_i}\frac{\partial p}{\partial \xi_j}+\frac{1}{\mathrm{Re}}\left(\frac{\partial \xi_j}{\partial x_l}\frac{\partial \xi_k}{\partial x_l}\frac{\partial^2}{\partial \xi_i \partial \xi_k}+\frac{\partial^2}{\partial x_l \partial x_l}\frac{\partial}{\partial \xi_j}\right)u_i \tag{1}$$

$$\left(\frac{\partial \xi_j}{\partial x_i}\frac{\partial \xi_k}{\partial x_i}\frac{\partial^2}{\partial \xi_i \partial \xi_k}+\frac{\partial^2 \xi}{\partial x_i \partial x_i}\frac{\partial}{\partial \xi_j}\right)p=\frac{1}{\Delta t}\left(\frac{\partial \xi_j}{\partial x_i}\frac{\partial u_i}{\partial \xi_j}\right)-\frac{\partial \xi_k}{\partial x_i}\frac{\partial \xi_l}{\partial x_j}\frac{\partial u_j}{\partial \xi_k}\frac{\partial u_i}{\partial \xi_l}$$
$$+u_j\frac{\partial \xi_k}{\partial x_j}\frac{\partial}{\partial \xi_k}\left(\frac{\partial \xi_l}{\partial x_i}\frac{\partial u_i}{\partial \xi_l}\right)$$
$$+\frac{1}{\mathrm{Re}}\left(\frac{\partial \xi_j}{\partial x_i}\frac{\partial \xi_k}{\partial x_i}\frac{\partial^2}{\partial \xi_j \partial \xi_k}+\frac{\partial^2 \xi_j}{\partial x_i \partial x_i}\frac{\partial}{\partial \xi_j}\right)\left(\frac{\partial \xi_m}{\partial x_l}\frac{\partial u_l}{\partial \xi_m}\right) \tag{2}$$

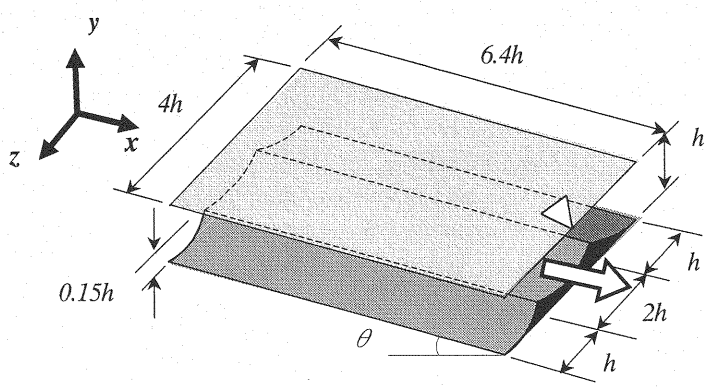

Fig. 1 : Computational domain

Table 1 Computational conditions

Coupling algorithm	Fractional Step Method
Time advancement	3rd Adams-Bashforth Method
Grid system	Regular Grid System
Spatial scheme	5th-order Upwind Scheme (Convective term) 4th-order Central Scheme (The others)
Grid numbers	64×65×65
Spatial resolution	Δx^+=14.7 (x^+= 942)
	Δy^+=0.1～5.8 (y^+=150)
	Δz^+=8.0～9.6 (z^+= 600)
Reynolds number	$Re_\tau = u_\tau h / \nu = 150$
Time step	$\Delta t = 2/1000 * h / u_\tau$

RESULTS AND DISCUSSION

An analytical study was conducted on the statistics obtained from three-dimensional turbulent fluctuations of 500,000 steps ($\cdot t = 2/1000*h/u_*\cdot$) in a fully developed turbulent flow field. Time-space averaged friction velocity $<u_*>$ was used to make the statistics dimensionless.

Figure 2 shows the vertical distribution of mean velocity U^+ where y^+ represents the height from the bed surface at each position. The figure clearly shows a large differences in mean streamwise velocities owing to the effects of ridges and troughs. While the distribution of velocities over ridges (z/h=1 and 3) agree with the distribution governed by the logarithmic law as in flat open channel flows, the distribution over troughs (z/h=0, 2 and 4) shifts toward higher velocities in the logarithmic region.

Figure 3 compares a computed cross-sectional distribution of friction velocities with the flume test results obtained by Nezu and Nakagawa [10]. Both show variations in the shear stress acting on the riverbed. The friction velocity had a minimum value on ridges and then increased gradually toward the troughs. While Nezu and Nakagawa regarded rough trapezoidal bars as ridges and evaluated friction velocity based on the logarithmic law, the authors computed friction velocity based on the velocity gradient on the bed surface. Despite such a difference in methods of the evaluation, both distributions generally agreed fairly well with each other.

Computed results of the mean velocity U^+ and the vectors of secondary currents (V^+,W^+) are shown in Fig. 4 and 5, respectively. Figure 4 shows that the mean velocity U^+ is high over the trough and low over the ridges. Figure 5 indicates that the downflow appears over the trough and upflow over the ridges. The effects of the secondary currents on the spatial distribution of main flow velocity is thus reproduced satisfactorily [8],[13].

Figure 6 shows isolines for vorticity ω_x^+. Longitudinal vortices at a scale of flow depth are aligned in mutually different rotational directions. The centers of longitudinal vortices do not match those of secondary currents, but are closer to the ridges. This is because the behavior is similar to that of longitudinal vortices generated in the viscous sublayer as shown by Smith and Schwartz [15]. In addition, the center of longitudinal

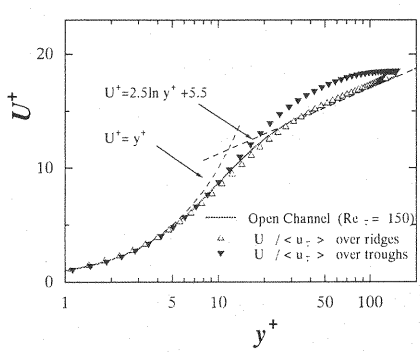

Fig. 2: Distribution of mean streamwise velocity

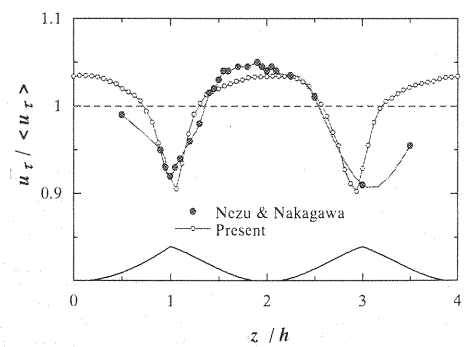

Fig. 3: Spanwise distribution of u

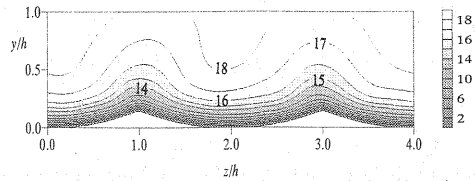

Fig. 4 Contours of mean streamwise velocity U^+

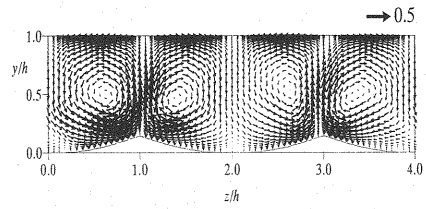

Fig. 5 Vectors of secondary currents V^+,W^+

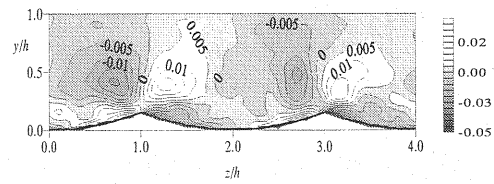

Fig. 6 Contours of vorticity ω_x^+

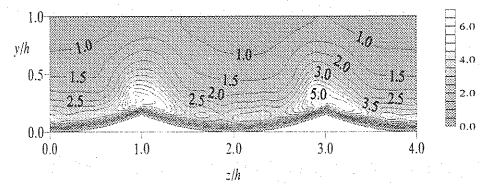

Fig. 7 Contours of turbulence energy k^+

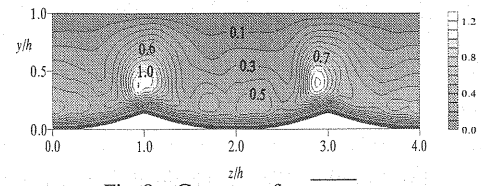

Fig. 8 Contours of $-\overline{u^+v^+}$

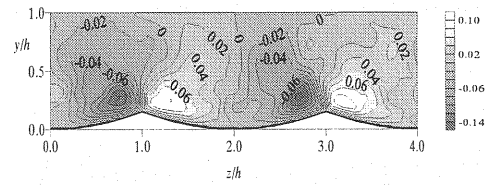

Fig. 9 Contours of $-\overline{v^+w^+}$

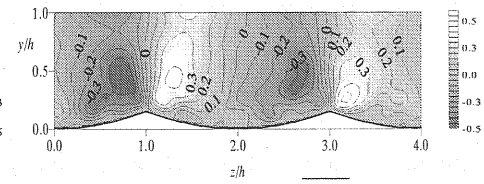

Fig. 10 Contours of $-\overline{u^+w^+}$

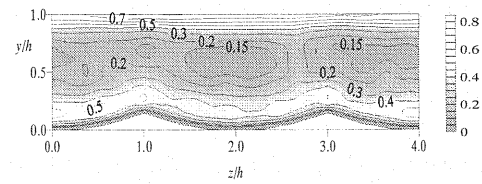

Fig. 11 Contours of $(\overline{w^{+2}}-\overline{v^{+2}})$

vortices approaches in such a direction as to cause to upflow owing the mutual action of vortices and to the effects of the bottom wall. Longitudinal vortices at a scale of flow depth, unlike those in the sublayer, have their centers near the bottom because of the effect of the free surface serving as a boundary. These reproduced phenomena agree with the results of stability analysis using a vortex filament model [14].

The computed turbulent statistics are shown in Figs.7 through 11. Turbulent energy k^+ is greatest over the ridges in the upflow region, and smallest over the troughs in the downflow region and its spatial distribution agrees well with the data obtained by measurements [8].

The relationship among the terms of Reynolds shear stress that rules the generation of turbulent energy is shown below.

$$\left|-\overline{u^+v^+}\right|_{\max} \cong 2\left|-\overline{u^+w^+}\right|_{\max} \cong 10\left|-\overline{v^+w^+}\right|_{\max}$$

$$\left|-\overline{u^+v^+}\frac{\partial U^+}{\partial y^+}\right|_{\max} \cong 10\left|-\overline{u^+w^+}\frac{\partial U^+}{\partial z^+}\right|_{\max} \cong 200\left|-\overline{v^+w^+}\frac{\partial W^+}{\partial y^+}\right|_{\max} \cong 250\left|-\overline{v^+w^+}\frac{\partial V^+}{\partial z^+}\right|_{\max}$$

For the generation of turbulent kinetic energy, $-\overline{u^+v^+}$ and $-\overline{u^+w^+}$ are the dominant terms and $-\overline{v^+w^+}$ can be ignored. $(\overline{w^{+2}}-\overline{v^{+2}})$ representing anisotropy of turbulence has a large positive value near the free-surface and the bed, thus indicates higher anisotropy due to the constraint on $\overline{v^{+2}}$ at the boundary. and $(\overline{w^{+2}}-\overline{v^{+2}})$ slightly decreases cross-sectionally over the trough. The turbulent kinetic energy budget in the flow field where stable secondary currents exist is shown by equation (3) below.

$$U_j^+\frac{\partial}{\partial x_j}\left(\overline{\frac{u_i^+u_i^+}{2}}\right)=-\frac{\partial}{\partial x_j}\left(\overline{u_j^+p^+}+\overline{\frac{u_i^+u_i^+u_j^+}{2}}-\frac{2}{\mathrm{Re}_\tau}\overline{u_i^+s_{ij}^+}\right)-\overline{u_i^+u_j^+}S_{ij}^+ -\frac{2}{\mathrm{Re}_\tau}\overline{s_{ij}^+s_{ij}^+} \tag{3}$$

$$\text{where}\quad s_{ij}^+\equiv\frac{1}{2}\left(\frac{\partial u_i^+}{\partial x_j}+\frac{\partial u_j^+}{\partial x_i}\right),\qquad S_{ij}^+\equiv\frac{1}{2}\left(\frac{\partial U_i^+}{\partial x_j}+\frac{\partial U_j^+}{\partial x_i}\right)$$

In equation(3), the convection term of turbulent kinetic energy generated by secondary currents is on the left-hand side, and the first, second and third terms on the right-hand side are the diffusion, the production and the dissipation terms, respectively. The vertical distributions of each term over the ridges and the toughs where turbulent kinetic energy exhibit maximum and minimum values are shown in Fig. 12. For comparison, the figure also plots the computational results for flows between parallel plates carried out by DNS [7]. A comparison made for each term in the turbulent kinetic energy budget equation between flows over a bed with ridges where secondary currents developed and flows between parallel plates shows no significant difference except for the production and turbulent diffusion terms over the ridges. The turbulence production term is greater over the ridges because $-\overline{u^+v^+}$ in the Reynolds shear stress is extremely large near the ridges as is obvious from Figs.8 and 13. It should be noted that the turbulent diffusion term is also different from that for flows between parallel plates because the secondary currents have an impact on high-order, specifically third-order moments.

The effects of secondary currents on the Reynolds shear stress were examined by using equation (4) as determined by Nakagawa, Nezu & Tominaga [9], which was obtained by vertical integration of the Reynolds momentum equation in the mainstream direction where h is the flow depth.

$$-\overline{u^+v^+}+\frac{1}{\mathrm{Re}_\tau}\frac{\partial U^+}{\partial y}=\left(1-\frac{y}{h}\right)-\int_y^h\left(V^+\frac{\partial U^+}{\partial y}+W^+\frac{\partial U^+}{\partial z}\right)dy +\int_y^h\frac{\partial}{\partial z}\left(-\overline{u^+w^+}\right)dy \tag{4}$$

In a two-dimensional uniform flow field, the turbulent shear stress exhibits a linear

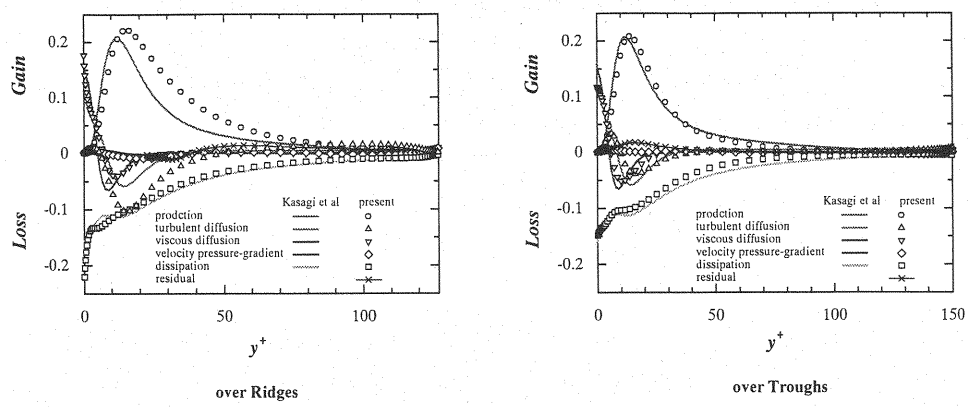

Fig.12:Budget of turbulent kinetic energy

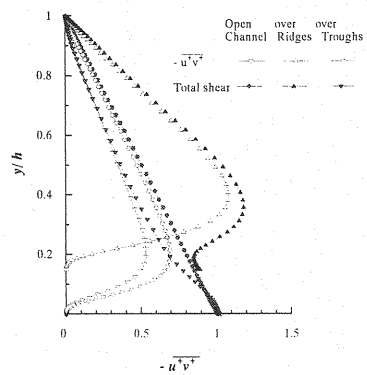

Fig.13: Turbulent shear stress

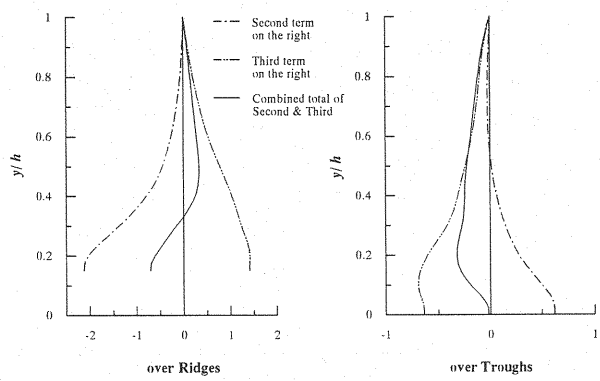

Fig.14:Integration of additional stress terms of the momentum equation

distribution due to the first term on the right-hand side. In a flow field with secondary currents, however, a convection term (second term on the right-hand side), and a turbulent diffusion term (third term on the right-hand side) are added to the turbulent shear stress. The computational results of the second and third terms on the right-hand side over the ridges and troughs are shown in Fig. 14. The second term on the right-hand side weakens the shear stress in the upflow region, and strengthens it in the downflow region. It is evident that the third term on the right-hand side, indicating the cross-sectional momentum transport due to turbulence $-\overline{u^+w^+}$, has a sign opposite to that of the second term, and thus strengthens the shear stress over ridges and weakens it over troughs. The total of the second and third terms on the right-hand side has the maximum and minimum values over ridges near y/h = 0.4 and 0.15, respectively. Whereas the total over troughs has the minimum value near y/h=0.2. This explains the spatial distribution of Reynolds shear stress as shown in Figs.8 and 13 and is consonant with the fact that the shear stress at the bottom is small in the upflow region, and large in the downflow region [8][13].

GENERATION MECHANISM OF SECONDARY CURRENTS

Based on the work of Brundrett et al. [2], the mean vorticity equation is expressed by equation (5) where ω_x^+ is a mean streamwise voriticity .

$$U_j^+ \frac{\partial \omega_x^+}{\partial x_j} = \frac{\partial^2}{\partial y \partial z}(\overline{v^{+2}} - \overline{w^{+2}}) + (\frac{\partial^2}{\partial y^2} - \frac{\partial^2}{\partial z^2})(-\overline{v^+ w^+}) + \frac{1}{\mathrm{Re}_\tau}(\frac{\partial^2}{\partial y^2} + \frac{\partial^2}{\partial z^2})\omega_x^+ \quad (5)$$

Computed values of the convection term on the left-hand side and the difference of Reynolds normal stress (the first term), Reynolds shear stress (the second term), and viscous diffusion (the third term) are shown in Fig. 15. The values agreed fairly well with the experimental results conducted by Nezu and Nakagawa [11]. In the regions with a high absolute value of ω_x^+, the second and third terms on the right-hand side are predominant and have opposite signs to achieve balance. Convection and viscous diffusion terms are relatively small, so they can be ignored. As shown in Fig.8 ~ Fig.10, the Reynolds shear stress $-\overline{v^+ w^+}$ is much smaller than the other Reynolds shear stress terms, and can be ignored in the turbulent energy budget. However, the spatial second-order derivative is relatively large and is also the dominant term in the balance equation of ω_x^+. It was observed that the sign of ω_x^+ is the same as that of the spatial second-order derivative of the Reynolds shear stress $-\overline{v^+ w^+}$, but opposite to that of the spatial second-order derivative of the difference of the Reynolds normal stress $(\overline{v^{+2}} - \overline{w^{+2}})$. Therefore, the computational results based on DNS showed that while the difference of Reynolds normal stress $(\overline{v^{+2}} - \overline{w^{+2}})$, which has been conventionally believed to generate secondary currents, depresses secondary currents, the Reynolds shear stress $-\overline{v^+ w^+}$ drives the generation of secondary currents and that secondary currents were stably balanced by them.

CONCLUSIONS

1) DNS satisfactorily reproduced the flow field over a riverbed with longitudinal ridges because the computational results were in good agreement with experimental results with respect to turbulence statistics such as the mean velocity, the Reynolds shear stress, and the mean streamwise vorticity.
2) The turbulent kinetic energy budget was investigated over ridges and troughs. Over troughs, each term in the turbulent kinetic energy budget equation agreed with that of flows between parallel plates. Over ridges, however, the production and turbulent diffusion terms of the equation energy were affected by secondary currents and different from those in flows between parallel plates.
3) The effects of secondary currents on the Reynolds shear stress $-\overline{u^+ v^+}$ were examined

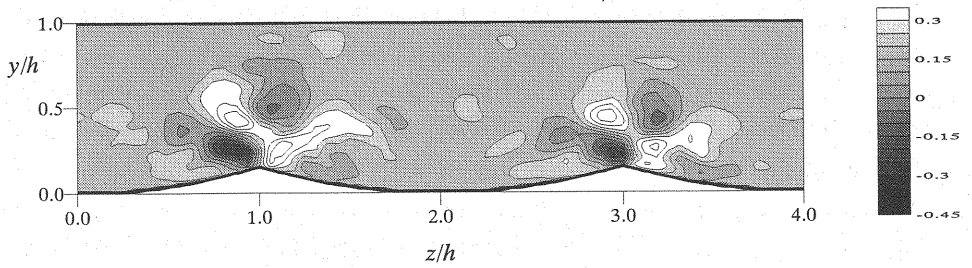

(A) convection terms $(V^+\frac{\partial \omega_x^+}{\partial y^+}+W^+\frac{\partial \omega_x^+}{\partial z^+})\times 10^3$

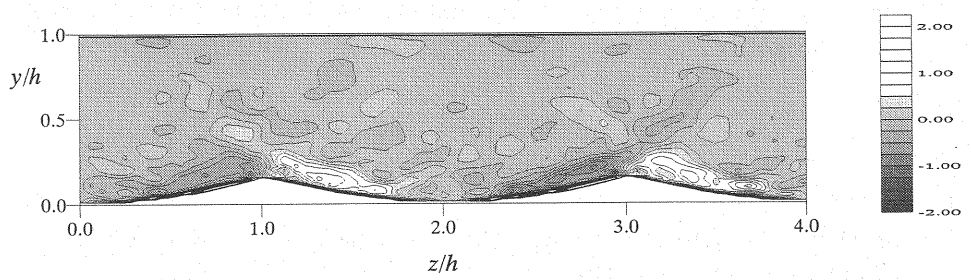

(B) Reynolds normal-stress terms $\frac{\partial^2}{\partial y^+\partial z^+}(\overline{v^{+2}}-\overline{w^{+2}})\times 10^3$

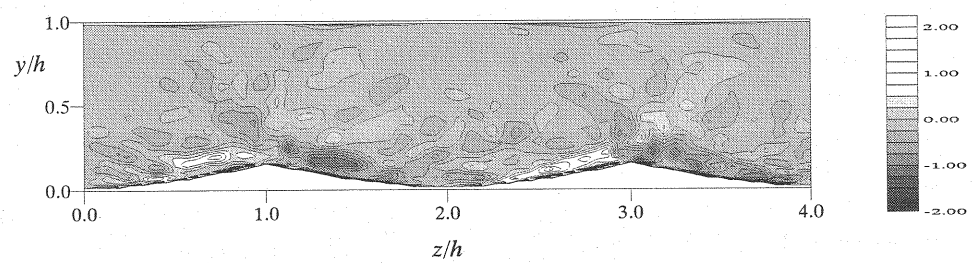

(C) Reynolds shear-stress terms $(\frac{\partial^2}{\partial z^{+2}}-\frac{\partial^2}{\partial y^{+2}})\overline{v^+w^+}\times 10^3$

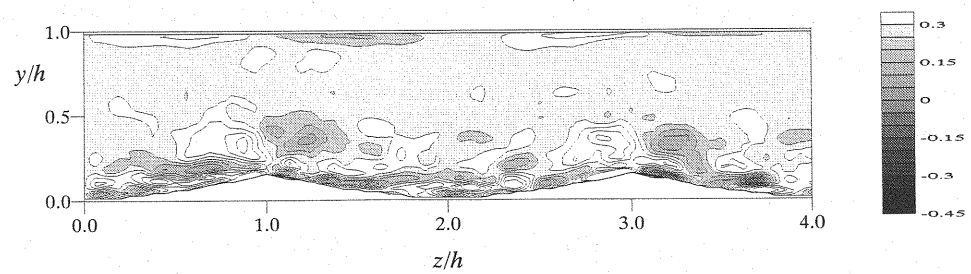

(D) viscous diffusion term $\frac{1}{\mathrm{Re}_\tau}(\frac{\partial^2\omega_x^+}{\partial y^{+2}}+\frac{\partial^2\omega_x^+}{\partial z^{+2}})\times 10^3$

Fig.15: Contours of each term of the mean streamwise vorticity transport equation

by using a momentum transport equation. Findings showed that the wall shear stress is large near troughs and small near ridges due to the tendency of upflows to weaken and downflow to strengthen $-\overline{u^+v^+}$. In addition, the cross-sectional momentum transport due to turbulence $-\overline{u^+w^+}$ strengthens $-\overline{u^+v^+}$ over troughs and weakens it over ridges.

4) The generation mechanism of secondary currents was studied by using the mean streamwise vorticity equation. Results showed that while the difference of the Reynolds normal stress $\overline{v^{+2}}-\overline{w^{+2}}$ attenuates secondary currents, the Reynolds shear stress $-\overline{v^+w^+}$ is the main cause of secondary currents and therefore drives the generation of secondary currents. Thus balance between the Reynolds shear stress $-\overline{v^+w^+}$ and normal stress $\overline{v^{+2}}-\overline{w^{+2}}$ generates stable secondary currents over the longitudinal ridges.

REFERENCES

1. Bradshaw,P. : Turbulent secondary flows, *Ann.Rev. Fluid Mech.*, No.19, pp.53-74, 1987.
2. Brundrett,E. and Baines,W.D. : The production and diffusion of vorticity in duct flow, J. Fluids Mech., Vol.19, pp. 375-394, 1964.
3. Hayashi,S., Ohmoto,T., Yakita,K.and Hirakawa,R. : Direct numerical simulation of open channel turbulence using generalized coordinate system and upwind difference scheme, J.of Applied Mechanics, JSCE, Vol. 2, pp.599-608, 1999. (in Japanese)
4. Hayashi,S., Ohmoto,T.and Takikawa,K. : Fundamental study on direct numerical simulation using a high-order accuracy upwind diference scheme, J.of Hydroscience and Hydraulic Eng., JSCE, Vol. 19, No.2, pp.93-104, 2001.
5. Hayashi,S., Ohmoto,T.and Hirakawa,R. : Direct numerical simulation of open-channel turbulent flow using a regular grid in a generalized coordinate system, J.of Hydroscience and Hydraulic Eng., JSCE, Vol. 19, No.1, pp.65-74, 2001.
6. Huser,A and Biringen,S : Direct numerical simulation of turbulent flow in a square duct, *J. Fluid Mech.*, Vol.257, pp.65-95, 1993.
7. Kuroda,A.and Kasagi,N. : Establishment of the direct numerical simulation data base of turbulent transport phenomena, Co-operative Research, Ministry of education science and culture, 1992. (in Japanese)
8. Nakagawa,H., Nezu,I. and Tominaga,K. : Turbulent structure with cellular secondary flow, J. of Hydraulic Eng., JSCE,Vol.26, pp.469-474, 1982. (in Japanese)
9. Nezu,I. and Nakagawa.,H. : Turbulence in Open- Channel Flows, IAHR - Monograph, Balkema, 1993.
10. Nezu,I. and Nakagawa,H. : Cellular secondary currents in straight conduit, J. Hydraulic Eng., ASCE, Vol.110, No.2, pp.173-193, 1982.
11. Nezu,I. and Nakagawa,H. : Experimental study on cellular secondary currents by vorticity equation, J. Hydraulic Eng., JSCE, Vol.26, pp.641-646, 1982. (in Japanese)
12. Ohmoto,T. and Hirano,M. : Study on formation region of sand ribbons and characteristics of tractive force distribution, Proceedings of JSCE, No.399/II-10, pp.75-841, 1988. (in

Japanese)

13. Ohmoto,T.,Hirano,M. and Pallu,M.S. : Three-dimensional turbulent shear flow structure over sand ribbons, J. Hydraulic Eng., JSCE, Vol.33, pp.529-534, 1989. (in Japanese)
14. Ohmoto,T. and Hirano,M. : Stability mechanism and control of longitudinal vortex stress, J. Hydraulic Eng., JSCE, Vol.37, pp.495-501, 1993. (in Japanese)
15. Smith,C.R. and Schwartz,S.P. : Observation of streamwise rotation in the near-wall region of a turbulent boundary layer, Phys. Fluids, 26, No.3, pp.641-652, 1983.

APPENDIX – NOTATION

The following symbols are used in this paper :

h = flow depth ;
k^+ = turbulent kinetic energy ;
p = pressure ;
Re_τ = Reynolds number based on the friction velocity ;
s_{ij} = instantaneous velocity-gradient tensor ;
S_{ij} = mean velocity-gradient tensor ;
t = time ;
u_τ = friction velocity ;
u,v,w = instantaneous velocities in the x,y and z directions ;
$-\overline{u^+v^+}, -\overline{v^+w^+}, -\overline{u^+w^+}$ = dimensionless Reynolds shear stress
U,V,W = mean velocities in the x,y and z directions ;
$\overline{v^{+2}} - \overline{w^{+2}}$ = difference of Reynolds normal stress
x,y,z = coordinates of the streamwise,vertical and spanwise directions ;
Δt = time increment ;
$\Delta x, \Delta y, \Delta z$ = grid spacings in the x,y and z directions ;
$\Delta x^+, \Delta y^+, \Delta z^+$ = grid spacings in wall units in the coordinate x,y and z directions ;
δ = channel half-width ;
ξ_i = coordinates in calculation space ; and
ω_x^+ = dimensionless mean vorticity.

+(superscript) = non-dimensional coordinate normalized by the viscous length.

(Received July 18, 2002 ; revised March 19, 2003)